

Experimental and numerical studies on cyclic behavior of continuous-tenon joints in column-and-tie timber construction

Liangjie Qi^{1,2,3a}, Jianyang Xue^{*1,2} and Dan Xu^{1,2}

¹School of Civil Engineering, Xi'an University of Architecture & Technology, Xi'an 710055, China

²Key Lab of Structural Engineering and Earthquake Resistance, Ministry of Education (XAUAT), Xi'an 710055, China

³Disaster Prevention Research Institute, Kyoto University, Kyoto 6110011, Japan

(Received August 23, 2019, Revised March 5, 2020, Accepted March 12, 2020)

Abstract. The mechanical properties of timber construction have drawn more attention after the 2013 Lushan earthquake. A strong desire to preserve this ancient architectural styles has sprung up in recent years, especially for residential buildings of the mountainous areas. In the column-and-tie timber construction, continuous-tenon joints are the most common structural form to connect the chuanfang (similar to the beam in conventional structures) and the column. To study the cyclic performance of the continuous-tenon joints in column-and-tie timber construction, the reversed lateral cyclic loading tests were carried out on three 3/4 scale specimens with different section heights of the chuanfang. The mechanical behavior was assessed by studying the ultimate bending capacity, deformation ductility and energy dissipation capacity. Test results showed that the slippage of chuanfang occurred when the specimens entered the plastic stage, and the slippage degree increased with the increase of the section height of chuanfang. An obvious plastic deformation of the chuanfang occurred due to the mutual squeezing between the column and chuanfang. A significant pinching was observed on the bending moment-rotation curves, and it was more pronounced as the section height of chuanfang increased. The further numerical investigations showed that the flexural capacity and initial stiffness of the continuous-tenon joints increased with the increase of friction coefficient between the chuanfang and the column, and a more obvious increasing of bending moment occurred after the material yielding. The compressive strength perpendicular to grain of the material played a more significant role in the ultimate bending capacity of continuous-tenon joints than the compressive strength parallel to grain.

Keywords: column-and-tie timber construction; continuous-tenon joints; cyclic performance; parametric investigation; energy dissipation capability

1. Introduction

A great number of ancient timber structures still exist worldwide at the moment, especially in China, Japan and Canada, etc. In general, the wooden frame is the main structural skeleton, which bears the weight of the roof or floor, and partition walls only sustain its own weight at the same time. To meet the human living demands of spacious areas, sometimes no partition wall is present inside the house. According to the recent 2013 Lushan earthquake in rural China (Qu *et al.* 2015), the timber frame in the residential house has good mechanical properties in terms of structural function. Therefore, the seismic performance of this long-term surviving buildings can be summarized as "though the partition walls collapse, the main structure stands" (Zhao *et al.* 2012, Pan *et al.* 2017, Vieux-Champagne *et al.* 2017).

The existing Chinese traditional timber structures are mainly divided into two categories (Yue 2014). The first configuration, so-called post-and-lintel construction, is mainly built in the northern region of China, which is

mostly used for official and landmark buildings, as shown in Fig. 1(a); while the other one, the column-and-tie structures, are mostly located in southern China, employed as the common residential buildings (Fig. 1(b)). For post-and-lintel structures, not all of the columns stand on the ground, and short columns are often located on the upper surface of the chuanfang. The chuanfang is similar to the beam in conventional structures, illustrated in Fig. 1(a). Nevertheless, the bottom of every column in column-and-tie timber construction is connected to the ground, and the chuanfang often pass through the drilled holes in the columns (Fig. 2(b)), which are different extraordinarily compared with the post-and-lintel construction.

A great number of traditional wooden structures have not been maintained or repaired as they used to construct because of various reasons. Significant damage, such as wood decay and pull-out of tenon, existed under the extraneous influence of natural disasters or human activities, which threatens the structural integrity (Fang *et al.* 2001, Zhang *et al.* 2011). In recent years, some scholars have carried out researches on ancient timber structures through field investigations and structural experiments, laying a certain foundation for the detailed study of column-and-tie construction. Two full-scale specimens were fabricated and tested under cyclic lateral loading based on extensive investigation of residential houses by Guo (2016). The load-displacement curves of wood frames and moment-rotation

*Corresponding author, Professor, Ph.D.

E-mail: jianyang_xue@163.com

^a Associate professor, Ph.D.

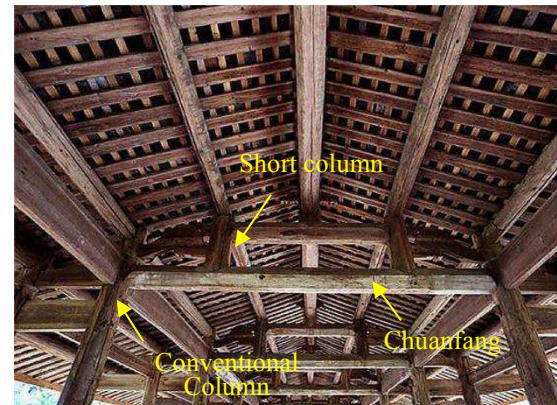
Email: qiliangjie@gmail.com

hysteric behavior of mortise-tenon joints were assessed. Test results showed that the slippage aggravated with the increase of the loading displacement, and the pull-out deformation of the joints dissipated most of the seismic energy. Hao (2015) explored the mechanical properties of post-and-lintel and column-and-tie timber construction by shake table test. Test phenomena showed that main damage form is the pull-out of tenon, the self-deformation of chuanfang and column is relatively negligible, no macroscopic compression failure of the structural members occurred. Xue *et al.* (2018, 2019) studied the seismic performance of Chinese traditional column-and-tie timber structure by shake table tests, two 3D models, including one without infilled wallboard and the other with infilled wallboard, were fabricated and tested. The two models had large flexibility and deformability under a rare earthquake, and the wallboard played a key role in lateral stiffness and displacement response. Zhang (2019) established a simple mortise-tenon exterior joint model and an overall framework model for column-and-tie wooden buildings. The results showed that the global slip of the framework and slip of the column footing increased with the increase of the load.

The above studies of the overall structural frame showed that the major damage was concentrated on the mortise-tenon joint and it absorbed most of the seismic energy. In recent years, the research interest in different kinds of mortise-tenon joints has increased and much more component-level studied was performed (Chen *et al.* 2016, Yeo *et al.* 2016, Chen *et al.* 2017, Meng *et al.* 2018, Xie *et al.* 2018, Yeo *et al.* 2018). Five dovetail mortise-tenon joints with different loose degrees have been experimentally and numerically studied by Li *et al.* (2016), the test results demonstrated that the tenon was partially pulled out and the severe squeezing deformation occurred between the tenon and mortise. The ultimate bending capacity of dovetail joint degraded with the increase of the loose degree of joints. Apart from the dovetail mortise-tenon joints, Chun *et al.* (2011) studied the seismic performance of other four typical mortise-tenon joints in the Chinese southern timber buildings, including dovetail mortise-tenon joint, shizigitou mortise-tenon joint, half mortise-tenon joint and mantou mortise-tenon joint. The research results showed that the structural stiffness of dovetail mortise-tenon joint was the largest while mantou mortise-tenon joint had the lowest lateral stiffness.

The above-mentioned experimental researches are concentrated on various kinds of wood mortise-tenon joints, while there is still a lack of investigation on the cyclic behavior of continuous-tenon joints (Fig. 2). As described above, the chuanfang passing through the drilled holes in the column constitutes this kind of joint, and sometimes the orthogonal intersection of two continuous-tenon joints existed in practical engineering as well.

To investigate the cyclic behavior of continuous-tenon joints, a typical continuous-tenon joint from the conventional timber building in the southwestern region of China was taken as a prototype. Three specimens were subjected to combined constant axial load and vertical cyclic displacement loading; two actuators were employed to apply the vertical load oppositely and simultaneously at



(a) Post-and-lintel construction



(b) Column-and-tie construction

Fig. 1 Traditional timber structures

the two ends of chuanfang. The influence of section height of chuanfang (150 mm, 180 mm and 210mm) on the mechanical behaviors of continuous-tenon joints were analyzed in detail, and further parametric studies were performed to understand the effect of the coefficient of friction, compressive strength perpendicular to grain and compressive strength parallel to grain on structural initial stiffness and ultimate bending capacities. The experimental and numerical results are aimed to provide a theoretical basis for the structural design and analysis of continuous-tenon joints in the column-and-tie timber construction.

2. Experimental program

2.1 Test specimen

As shown in Fig. 2(b), the continuous-tenon joint is often cruciform-shaped with chuanfang directly passing through the column. According to the engineering practice of Chinese wooden dwellings, three 3/4 scale continuous-tenon joints with different section heights were designed and fabricated considering the limitation of the test field, named CTJ-1, CTJ-2, CTJ-3. The chuanfang was taken out between the bending inflection points and then loaded at the two endpoints. General dimensions of the specimens are given in Table 1. The wood material used in this project, *Cunninghamia lanceolata* (labeled henceforth as China fir), was the same as the practical traditional column-and-tie timber construction, its mechanical properties were tested

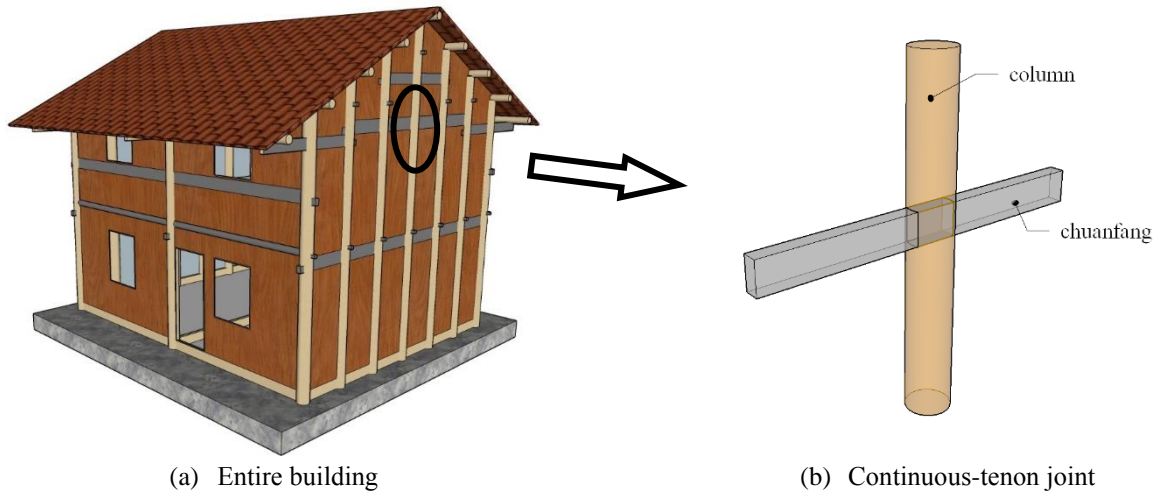


Fig. 2 Schematic diagram

Table 1 Dimensions of specimens

Specimen	Chuanfang (mm)			Column (mm)	
	Section height	Section width	Length	Diameter	Height
CTJ-1	150	60	2780	180	3520
CTJ-2	180	60	2780	180	3520
CTJ-3	210	60	2780	180	3520

Table 2 Mechanical properties of the material (MPa)

Tensile strength	Compressive strength parallel to wood grain	Compressive strength perpendicular to wood grain	Elastic modulus parallel to wood grain	Elastic modulus perpendicular to wood grain
55.15	30.16	3.73	6708	745

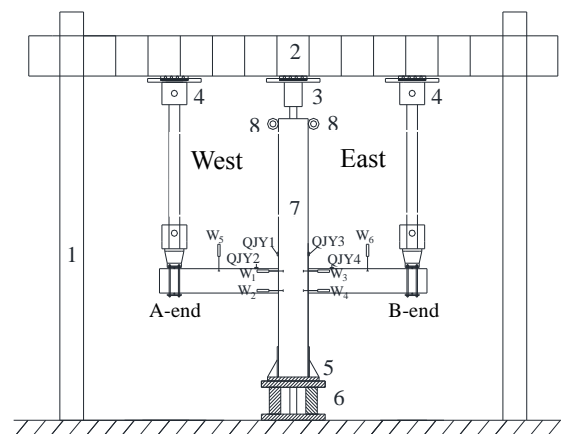
and measured based on GB/T 1929-09. Detailed mechanical properties are shown in Table 2. Note that all specimens were preserved by the plastic membrane before the loading test to avoid moisture evaporation.

2.2 Test scheme

The test rig is shown in Fig. 3. The bottom of the column was restricted by a steel sleeve to prevent the potential horizontal displacement of the column end, and a cantilever steel clamp was deployed to fix the column head.

The vertical constant load of 10 kN was applied to the column top, which was decided by the column axial force in actual structures considering the scale ratio, and then reversed cyclic loads was applied to the two ends of chuanfang by MTS973 electro-hydraulic servo systems. The two actuators applied the identical loading displacement oppositely within a stroke of ± 250 mm. Before the rotational angle at each end approaching 4%, cyclic loading was performed once every 0.5% angle increasingly, and then 2% increasing angle was cycled three times per level until the test was ended, as shown in Fig. 4.

The load and displacement at the loading point were measured by the force and displacement sensor of the actuator, four horizontal displacement transducers of W1 to W4 were used to measure the horizontal pull-out



1.Reaction frame 2. Reaction girder 3. Hydraulic jack 4. Actuators 5. Steel support 6. Foundation 7. Specimen 8. Clamp

Fig. 3 Test setup

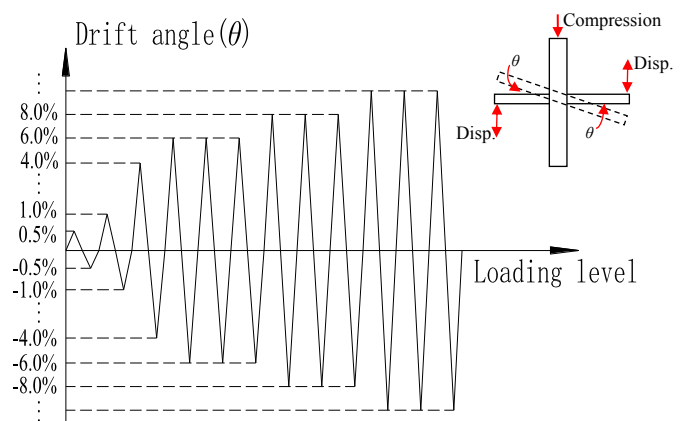


Fig. 4 Loading protocol

displacement between the mortise and tenon. Two vertical LVDTs, called W5 and W6, were placed 500mm away from the actuators to check the vertical displacement. The relative rotation angle between the column and chuanfang

on the left side of the joint was determined by the inclinometer QJY1, QJY2, and the corresponding rotation on the right side of the joint was measured by QJY3 and QJY4. The instrumentation plan is also shown in Fig. 3.

3. Results and discussion

3.1 Experimental phenomena

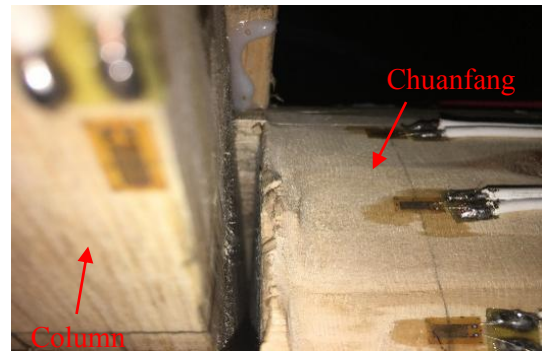
At the initial loading stage, the CTJ-1 specimen generated a small free rotation angle after being loaded, and then mortise and tenon squeezed with each other more obviously. When the drift angle reached 0.035 rad, the unrecoverable deformation on the chuanfang itself occurred by the squeezing and a small amount of pull-out of tenon existed. When the joint rotation exceeded 0.05 rad, there was a relatively large gap between the chuanfang and the mortise, indicating that the compressive deformation was non-negligible. As soon as the rotation angle reached 0.08 rad, the cracking of the wood occurred, the wood fiber tilted and the pull-out amount continued to increase. Cracks appeared on the upper surface at the west side of chuanfang when loading to 0.12 rad and the cracks extended to the east side at 0.16 rad rotation. But the column remained intact until 0.20 rad rotation and the deformation was too large to continue loading then. The deformation of CTJ-1 during the test are shown in Fig. 5.

The test phenomena of the CTJ-2 and CTJ-3 specimens were basically similar to that of the CTJ-1, except that the slippage between the column and chuanfang was more significant than that of the CTJ-1. Each joint had different degrees of free rotation due to the fabrication error or imperfection in the initial loading stage, the evident compressive deformation perpendicular to wood grain on the chuanfang and inapparent compressive deformation at the mortise occurred. A few cracks were generated on the surface of chuanfang around the mortise, and the wood fiber was continuously lifted and tilted, accompanied by the tearing noise of the timber itself. With the increase of reversed cyclic loads, a relatively large slippage of the chuanfang arised.

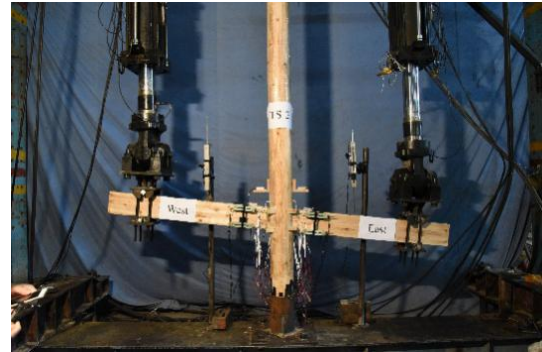
3.2 Hysteresis curves

Fig. 6 shows the hysteresis curves observed in the experiment, the last letter "A or B" represents A-end or B-end of chuanfang (Fig. 3). The bending moment is calculated by the product of applied force to the column center, and the rotation angle is measured by the corresponding inclinometers.

The pinching effect was obvious in the $M-\theta$ hysteresis curves, indicating that a large slippage was shown during the test. When the loading displacement was small, the bending moment of the joint increased slowly because the chuanfang and mortise were not tightened closely. When the loading angle exceeded 0.03 rad, the residual deformation existed after unloading, indicating that the joint entered the plastic phase. From the unloading curve at the maximum loading angle, the joint had undergone a large plastic deformation.



(a) Pull-out gap



(b) Ultimate deformation (0.22 rad)



(c) Tilting of the fiber around the mortise



(d) Compressive deformation of chuanfang

Fig. 5 Deformation of CTJ-1

By comparison, the hysteresis curves of A-end were not as full as B-end and the peak value was smaller at A-end. It was because of more pronounced pull-out and slippage at the A-end during the loading process, which can also be attributed to the slightly larger drilled mortise size of west side compared with the east side of the mortise (fabrication error). Different degrees of pinching were shown, the pinching phenomenon gradually aggravated as the

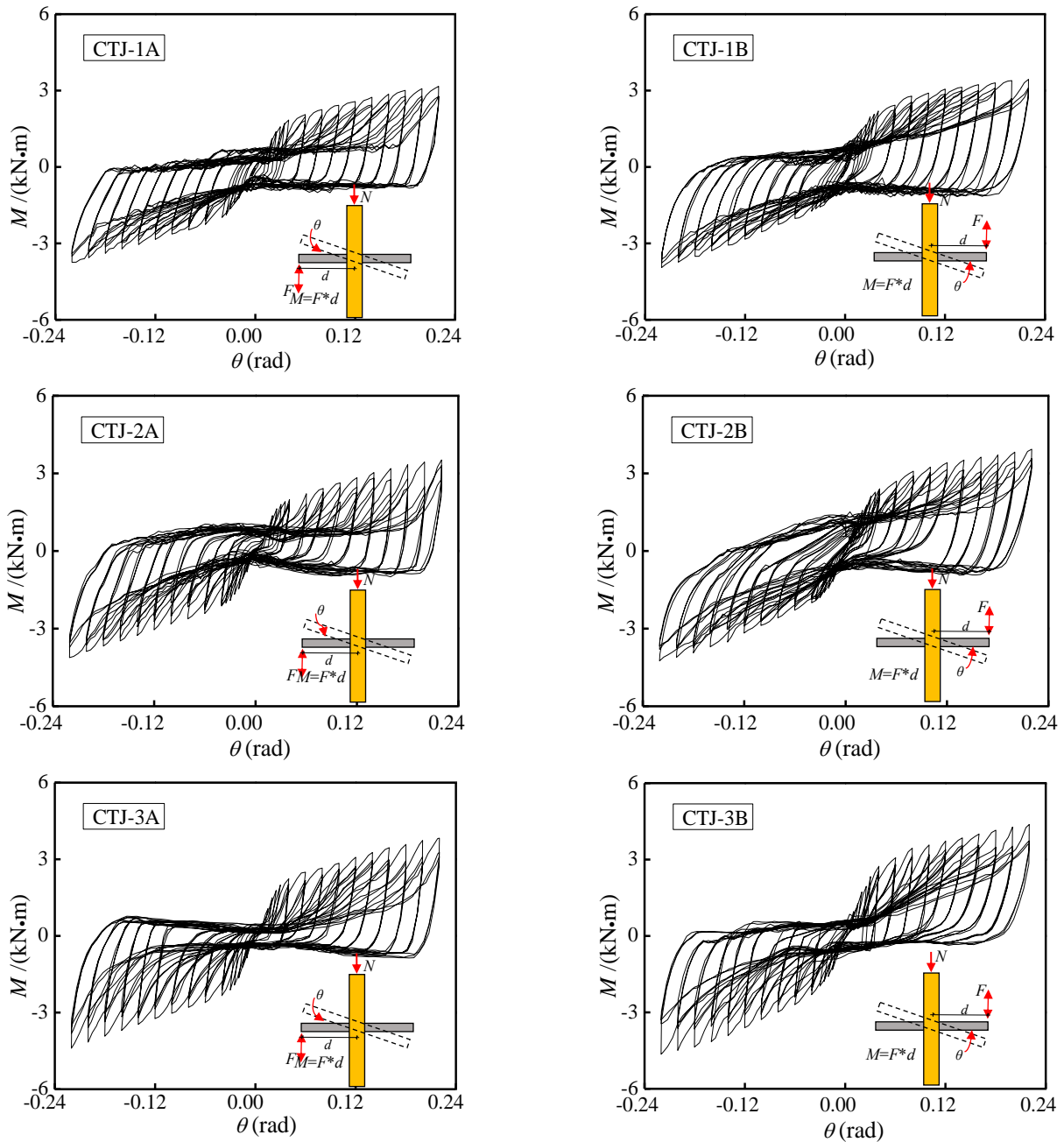


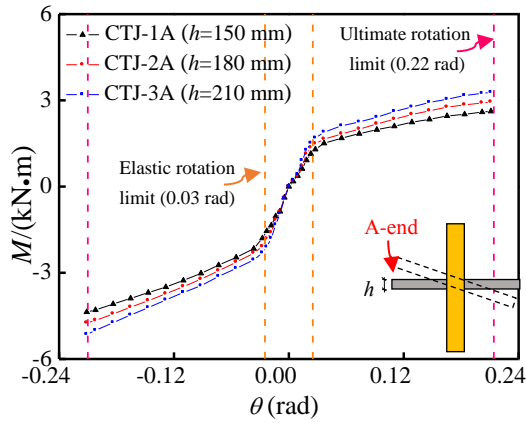
Fig. 6 Moment-rotation hysteretic loops

section height of chuanfang increased, indicating the more obvious slippage for larger stiffness specimens. Besides that, the fullness of the three test specimens decreased in turn as the section height of the chuanfang increased, indicating that the corresponding energy dissipation capacity was decreased continuously. This observation is due primarily to the smaller compressive deformation of larger stiffness specimen, nevertheless, the compressive deformation and squeezing of structural members dissipate most of the seismic energy.

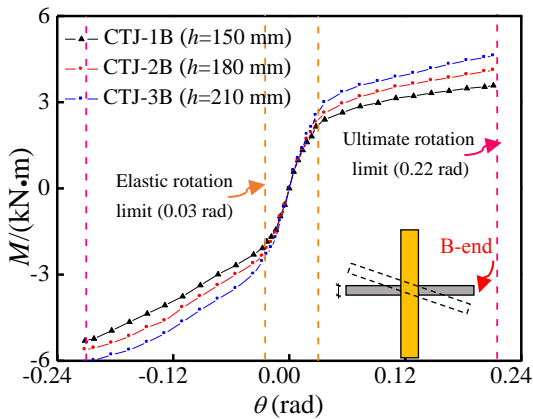
3.3 Backbone curves

The $M-\theta$ backbone curves are shown in Fig. 7. When the A-end actuator applied the downward load, the bending moment of the three specimens increased slowly under the

small loading angle. The reason was that there were initial gaps between the mortise and the tenon, and a certain free rotation existed at the initial loading stage; the measured load and displacement were basically linear, indicating that the test specimens were in the elastic working stage, and the elastic rotation limit was about 0.03 rad. As the loading angle continued to increase, the stiffness began to decrease and the joints entered the plastic stage. Because the strengthening of the wood material appeared when the perpendicular wood grain was in compression, the bearing capacity of the joint continued to increase until the end of loading. The load-bearing capacity of the joint did not decrease at the ultimate rotation limit (around 0.22 rad), which indicated that the continuous-tenon joint had the great deformability.



(a) A-end



(b) B-end

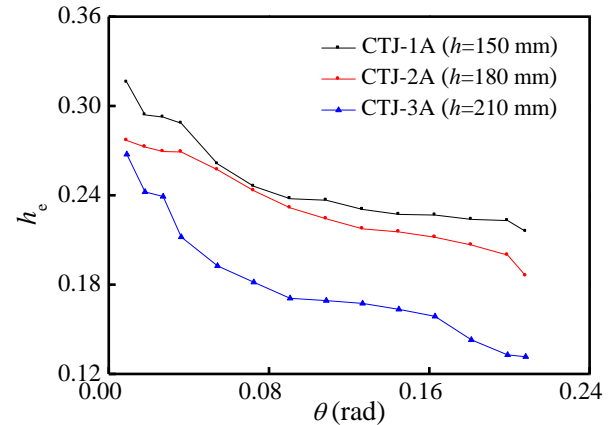
Fig. 7 Moment-rotation backbone curves

The variation law of backbone curves at A-end was consistent with B-end. Both the initial rotational stiffness and the bearing capacity of the joint increased with the increase of the section height of chuanfang, while the difference of elastic stiffness is not obvious due to the existence of the original gap between the mortise and the tenon. In addition, the bending capacity during positive loading is smaller than the reverse loading, thus the slightly larger original gap at west side of mortise than that of the east is confirmed as well by this observation.

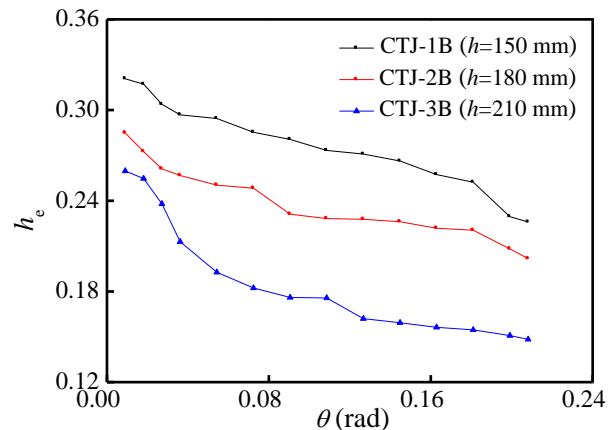
3.4 Ductility and energy dissipation

Ductility is an important index of structural seismic performance and it reflects the structural plastic deformability when the structure reaches the ultimate bearing capacity. The rotation angle limits for timber construction is usually set as 1/30 as per the standard GB 50165-92. From the above experimental results, the ultimate rotation of the continuous-tenon joint is over 0.2 rad (1/5), which is much larger than 1/30. This indicates that the continuous-tenon joints in column-and-tie timber construction have great deformability.

Energy dissipation ability is another measurement to evaluate the seismic performance of structural systems or components. It can directly reflect the structural ability absorbing and dissipating seismic energy during earthquakes. The results of the equivalent viscous damping



(a) A-end



(b) B-end

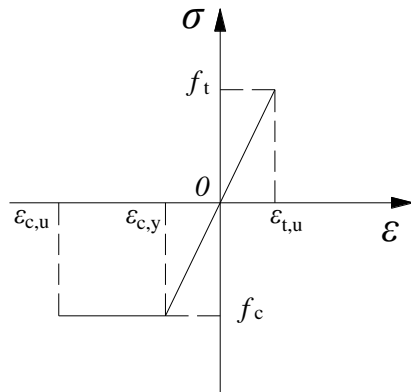
Fig. 8 Equivalent viscous damping coefficients

coefficient (h_e) (Xue *et al.* 2017) of each specimen are shown in Fig. 8.

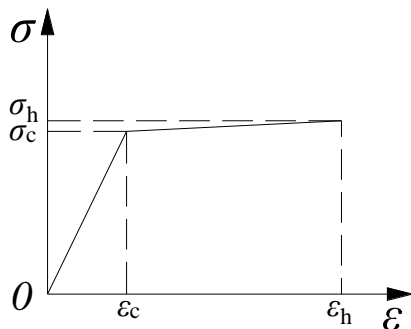
The following observations can be drawn based on Fig. 8.

(1) The equivalent viscous damping coefficients of the continuous-tenon joints are generally large, indicating that this kind of joint has the great energy dissipation capability. Before loading to 0.08 rad, the hysteresis energy dissipation coefficient decreased rapidly, and then relatively flat because the specimens experienced large plastic deformation in the late loading stage, and a large gap was generated between the mortise and chuanfang then. The more severe slippage and pinching effect result in a decrease of the areas of surrounded hysteresis loops, indicating the energy-dissipated value at each cycle was smaller than the previous level.

(2) Comparing the viscous damping coefficients of the three specimens, it is found that the viscous damping coefficient decreases gradually as the cross-section height of chuanfang increases, and the decreasing rate increases continuously, especially the significantly lowest viscous damping value for CTJ-3, indicating the energy dissipation capacity decreases with the increase of structural stiffness. The reason is that the compressive deformation of the chuanfang is less obvious but the slippage between the chuanfang and the column increases for the specimen with larger chuanfang (CTJ-3).



(a) Parallel to wood grain



(b) Perpendicular to wood grain

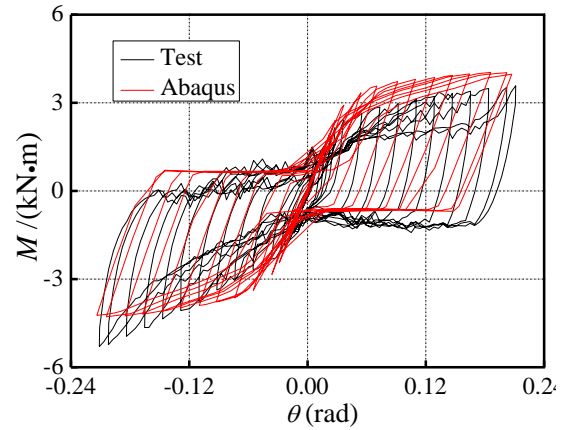
Fig. 9 Constitutive relationships of the material

4. Nonlinear cyclic analysis

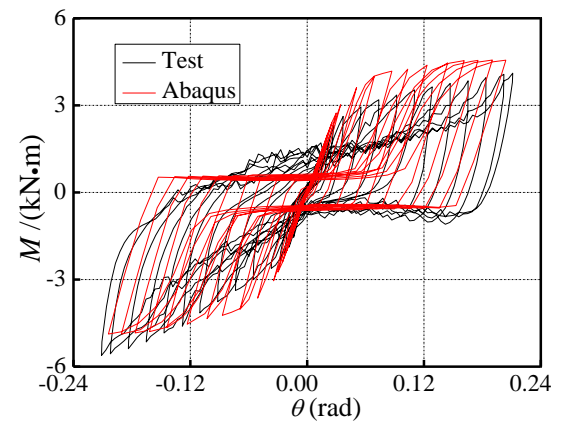
4.1 Finite element model construction

According to the actual size of the continuous-tenon joints in the aforementioned test, the ABAQUS finite element model was established. Eight-node solid reduced elements (C3D8R) and structured mesh were deployed in the model. The surface to surface contact method was adopted and the “hard contact” was used for normal direction between the chuanfang and the column, allowing the separation between column and chuanfang. Meanwhile, the penalty coefficient of 0.3 was used for tangential direction. The element mesh size of the master surface was smaller than that of the slave surface to prevent the face penetrating (Zhuang *et al.* 2009), the mesh size of the column was 20 mm and that of chuanfang was 30 mm.

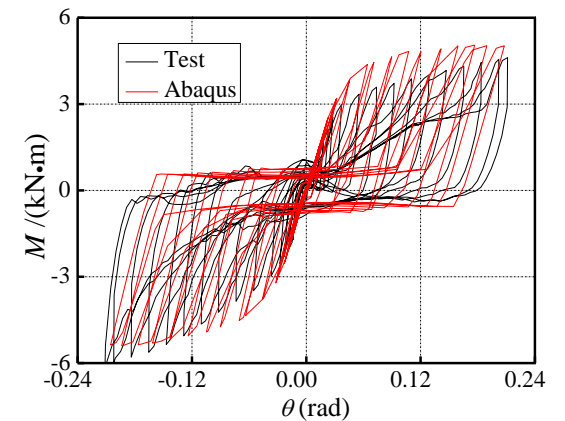
The properties of the material used here are the same as the experimental ones, determined by Engineering Constants in the ABAQUS software (Cui 2015). The Hill yield criterion of the anisotropic material was adopted. The constitutive relationship, including parallel and perpendicular to wood grain, is shown in Fig. 9, f_c and f_t denote the compressive and tensile strength parallel to wood grain, respectively; $\epsilon_{c,y}$, $\epsilon_{c,u}$, and $\epsilon_{t,u}$ are the compressive yield strain, compressive ultimate strain and ultimate tensile strain parallel to wood grain, respectively. σ_c and σ_h represent the compressive strength and ultimate strength perpendicular to the wood grain, ϵ_c and ϵ_h are the corresponding strains, respectively.



(a) CTJ-1



(b) CTJ-2



(c) CTJ-3

Fig. 10 Comparison of $M-\theta$ hysteresis curves

4.2 Validation of FE models

4.2.1 Comparisons of hysteretic loops

The comparisons of hysteresis curves between test and FEM are shown in Fig. 10. The hysteresis curves obtained from ABAQUS are similar to that of the test, and the pinching effect is obvious as well, which is consistent with the experimental one. As the section height of chuanfang increases, the area surrounded by the hysteresis loop under the same loading angle decreases, indicating that the hysteretic energy dissipation of the joint is weakened with larger stiffness specimen. In addition, the pinching

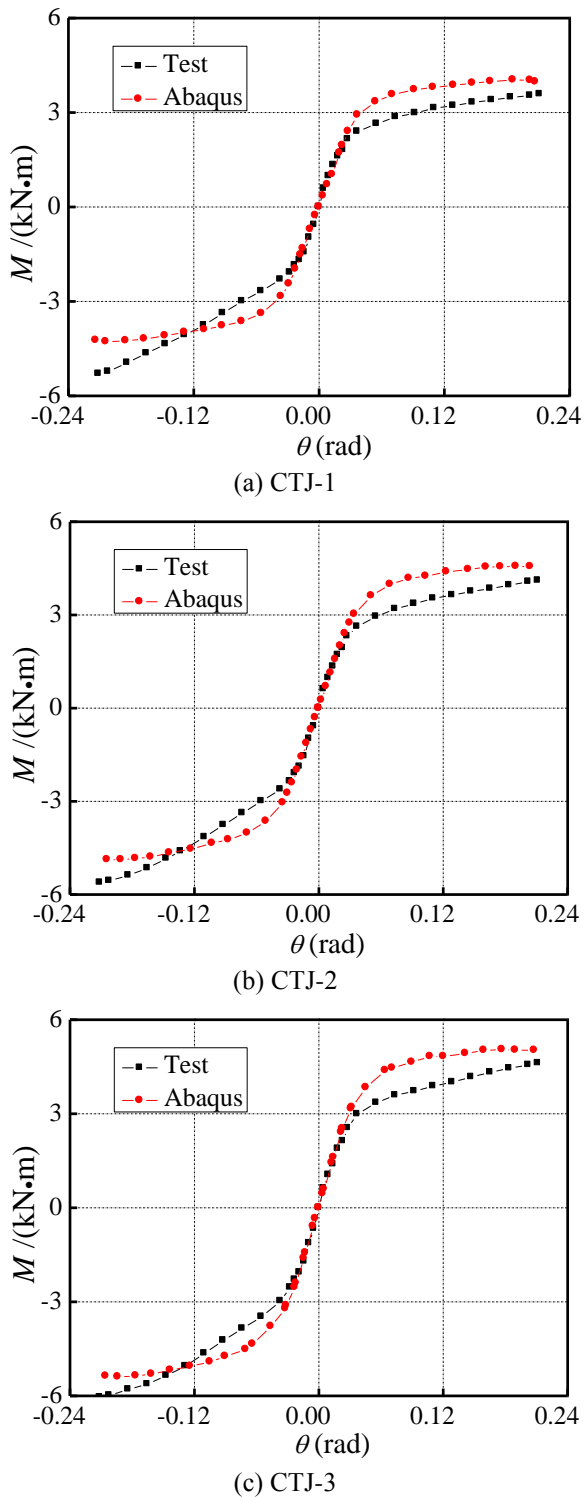


Fig. 11 Comparison of backbone curves

phenomenon of hysteresis loops is much more obvious with the larger chuanfang depth, which is due primarily to the large deformation and slippage of the chuanfang.

4.2.2 Comparisons of backbone curves

The comparisons of backbone curves between test and FEM are shown in Fig. 11.

In the elastic stage, the simulated value and the

experimental one are basically the same. Some differences appear between the two curves after the specimen enters the plastic stage. The first reason is that a large slippage occurred during the test results in asymmetrical loadings, so that the negative bending moment is greater than the positive bending moment in the tests. However, the simulation is in ideal condition, and numerical results are basically the same at both directions. On the other hand, the ideal elastoplastic model is used for compressive strength parallel to wood grain, while the actual wood has certain strengthening after yielding.

4.3 Stress distribution

4.3.1 Stress of chuanfang

Fig. 12 shows the stress contour of chuanfang at the ultimate rotation (0.22 rad). It can be seen from the S11 stress contour that the tensile and compressive stresses do not reach the tensile and compressive yield strength. Since the elastic modulus in compression perpendicular to wood grain is much smaller than parallel to the grain, the larger plastic deformation is produced in the perpendicular to the wood grain direction. From the S22 stress distribution figure, the compressive stress perpendicular to grain is greater than the tensile stress, the reason is that compressive deformations account for most of the deformation between chuanfang and mortise. The tensile stress occurs because the adjacent element is in compression status. Although the stress perpendicular to wood grain is larger than the compressive yield strength, no macroscopic damage occurs until the end of loading, which is consistent with the test results.

4.3.2 Stress of mortise

Fig. 13 shows the stress contour of the column when the positive loading reaches the maximum rotation angle. From S11 contours, the compressive and tensile stresses are much smaller than the tensile and compressive yield strength of the wood material. The deformation of the mortise is relatively small compared with the deformation of chuanfang, which is consistent with the deformation result of the mortise during the test. This is because the column compresses mainly in the parallel to grain direction, while the elastic modulus parallel to wood is much larger than that in the perpendicular to wood grain direction.

5. Further parametric investigations

5.1 Section height of chuanfang (h)

From the results of the above experiment, the section height of chuanfang plays a vital role in the mechanical characteristics of the joint. Because only three specimens were tested here, the variation range of parameters was relatively limited. Thus, two other configurations of 120 mm and 240 mm section height of chuanfang were further investigated.

In Fig. 14, the ultimate bending moment and the initial rotational stiffness of the joint model with the section height of 120 mm are smaller than those of the other joint

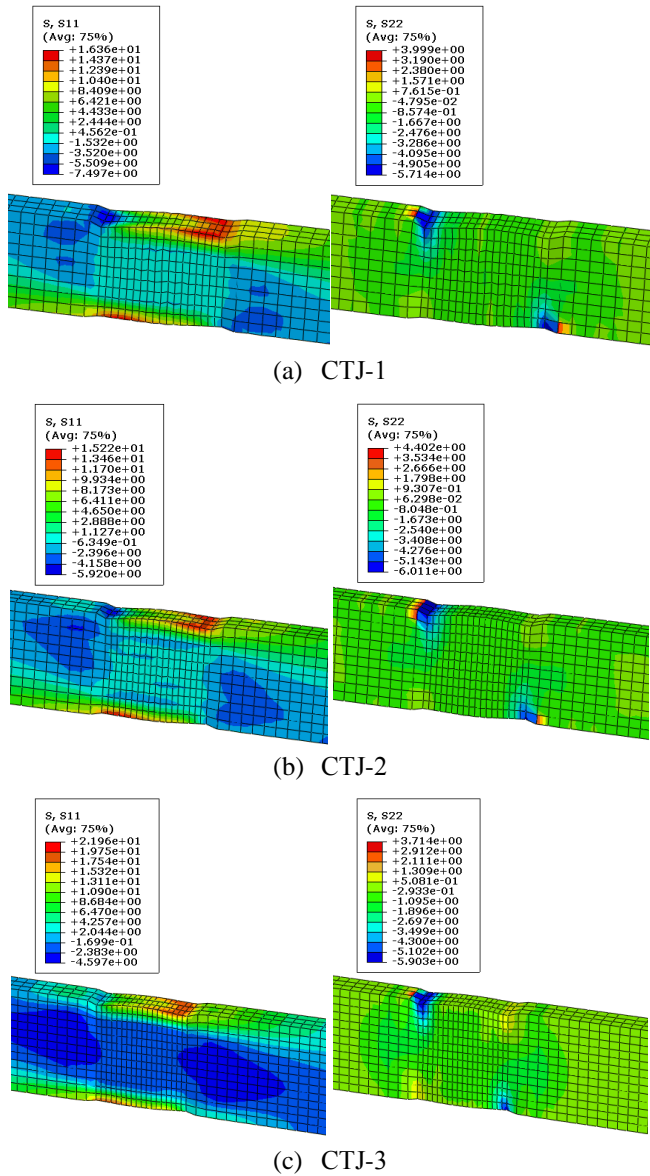


Fig. 12 Stress contour of chuanfang at ultimate rotation

models. When the section height of chuanfang is greater than 150mm, no significant increase is shown for the initial rotational stiffness. But the ultimate bending capacity increases continuously and the increase rate is almost uniform. The comparison results show that section height of chuanfang has a significant effect on the seismic performance of continuous-tenon joints in column-and-tie timber construction.

Besides that, the influence of section height on energy dissipation of continuous-tenon joints in column-and-tie timber construction is shown in Fig. 15. With the increasing of section height of chuanfang, the equivalent viscous damping coefficients decrease subsequently. The energy dissipation changes obviously as the chuanfang height is lower than 180 mm, while the equivalent viscous damping coefficients decrease slowly when the section height of chuanfang exceeds 180mm. It can be concluded that the identical height of chuanfang and the diameter of the column is a balanced configuration in terms of the ultimate

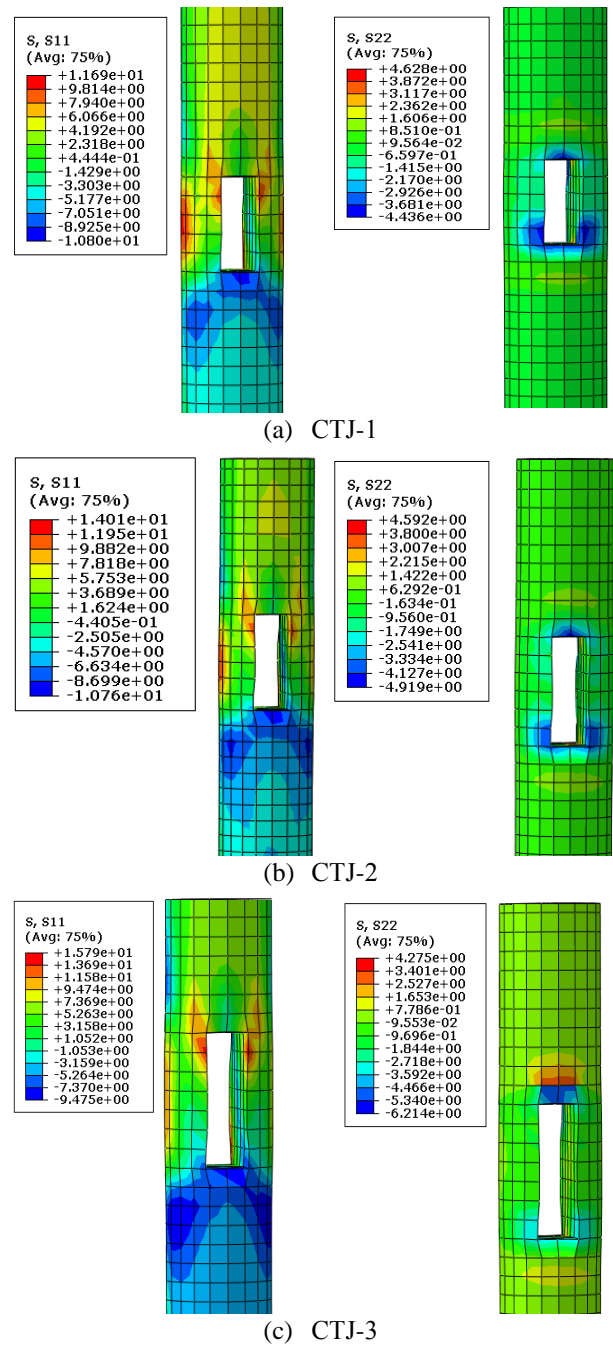


Fig. 13 Stress contour of mortise at ultimate rotation

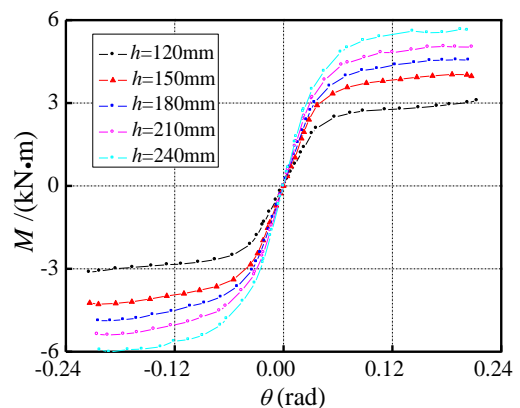


Fig. 14 The influence of section height of chuanfang on backbone curves

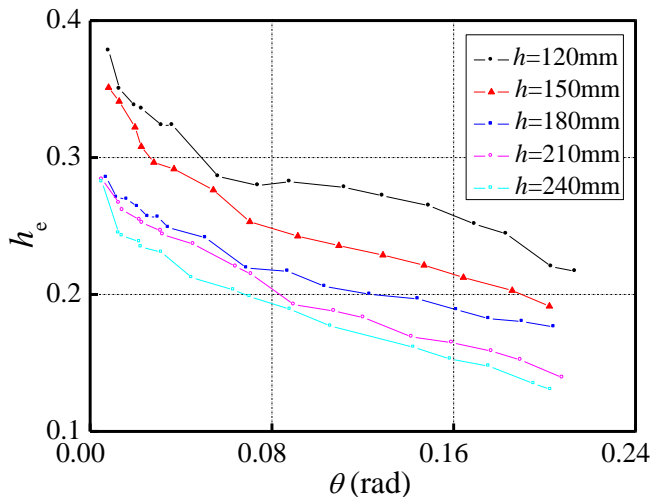


Fig. 15 The influence of section height of chuanfang on energy dissipation

bending capacity and the energy dissipation for the continuous-tenon joints.

5.2 Coefficient of friction (μ)

According to the existing research (McKenzie and Karpovich 1968, Murase 1984, Chen 2011), the friction coefficient of wood is within 0.1 to 0.6. The friction coefficients in this parametric study employ 0.3, 0.4, 0.5, and 0.6 to study its influence on the cyclic behavior of the continuous-tenon joint. The effects of different friction coefficients on the bending moment-rotation angle relationship of the joints are shown in Fig. 16.

In the elastic loading stage, the initial rotational stiffness of the joint increases with the increase of the friction coefficient, but the difference is nearly negligible. After the joint yielding, increasing the friction coefficient accelerates the increasing rate of the ultimate bending moment, which is more obvious than the elastic part. The friction characteristics mainly work at the surface contact between the chuanfang and the mortise. A significant compressive deformation occurs after the joints yield, resulting in a larger contact surface, which generates a greater influence of the coefficient of friction at the plastic stage than that of the elastic stage.

5.3 Compressive strength perpendicular to wood grain (σ_c)

During the rotation process, the restoring force is provided by the deformation of chuanfang in the perpendicular to grain direction. Therefore, the compressive strength perpendicular to wood grain is a key factor affecting the mechanical properties of the joints. The calculation is performed at 0.6, 0.8, 1.0, 1.2, and 1.4 times of experimental compressive strength perpendicular to wood grain (σ_c), and the FEM results are shown in Fig. 17.

As the compressive strength perpendicular to grain increases, there is no significant difference in the elastic stage. The bending moment increases obviously with the

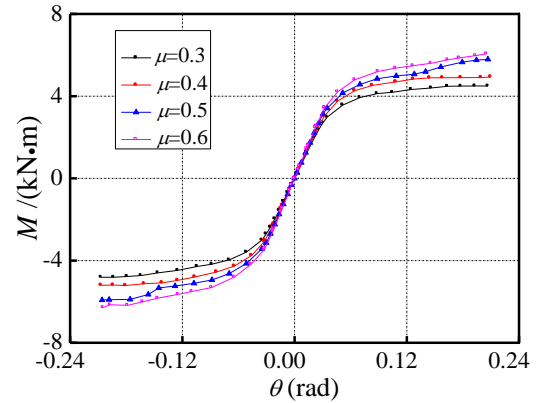


Fig. 16 The influence of friction coefficient on M- θ relationship

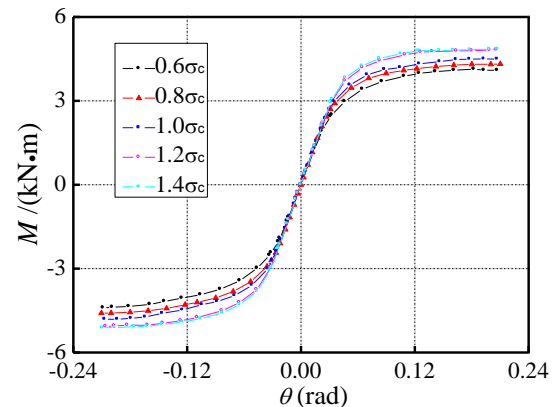


Fig. 17 The influence of compressive strength perpendicular to grain on backbone curves

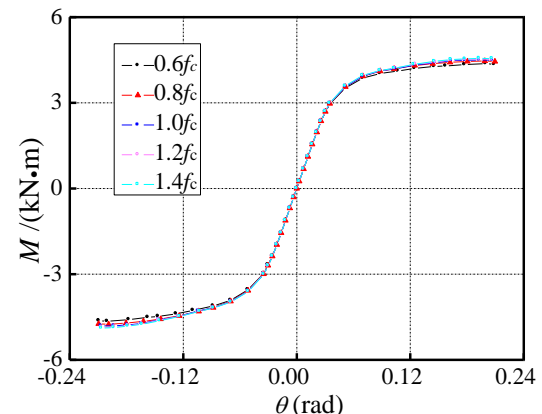


Fig. 18 The influence of compressive strength parallel to grain on backbone curves

increase of σ_c after the specimen enters the plastic stage. However, the two curves are almost the same when compared 1.2 σ_c and 1.4 σ_c results, representing that larger σ_c above experimental compressive strength perpendicular to grain is not really helpful to increase the bending capacity.

5.4 Compressive strength parallel to grain (f_c)

When the joints are subjected to external loads, the compression in parallel to grain direction takes place on the mortise. Thus, the influence of different compressive strength parallel to grain should be considered. The study is

performed at 0.6, 0.8, 1.0, 1.2, and 1.4 times of experimental compressive strength parallel to grain (f_c), as shown in Fig. 18.

As the compressive strength parallel to grain increases, almost no differences can be observed, indicating that the influence of f_c is smaller than that of σ_c . The reason is that the elastic modulus in compression parallel to wood grain is much larger than perpendicular to the wood grain direction. Moreover, the stress in parallel to the wood grain direction is smaller than stress in perpendicular direction. Until the end of the loading, the wood is still far from reaching its yield strength in the parallel to grain direction, representing a high strength reservation.

6. Conclusions

According to the above experimental and numerical results of the cyclic behavior of continuous-tenon joints in column-and-tie timber construction, the following conclusions can be addressed.

- A significant pinching was observed in the hysteresis curves of the continuous-tenon joints with different cross-section heights. The pinching degree is more obvious with the increase of the section height of chuanfang, indicating the significant slippage occurred during loading. The initial equivalent viscous damping coefficients of the joints decrease from 0.32 to 0.26 with section height increasing from 150 mm to 210 mm, indicating that the energy dissipation capacity is better for specimens with smaller stiffness of chuanfang.

- The ultimate rotation of the continuous-tenon joint is around 0.22 rad, far exceeding the rotation limit of 1/30 in the Chinese standard, indicating the rather excellent deformability for the continuous-tenon joints.

- With the increase of the friction coefficient between the chuanfang and the column, the bending capacity and initial stiffness of the continuous-tenon joints increase, and the post-yielding increasing degree is much more obvious than prior to yielding.

- No significant difference in the elastic stage is shown as the compressive strength perpendicular to grain increases. The increase of the compressive strength parallel to grain has almost no effect on the bending capacity and initial stiffness of continuous-tenon joints.

Acknowledgments

The authors would like to thank the support provided by the National Natural Science Foundation of China (Grant No. 51978568), Key Program of Basic Research on Natural Science of Shaanxi Province (Grant No. 2020JZ-50), and Shaanxi Key Scientific and Technological Innovation Team (Grant No. 2019TD-029).

References

Chen, C., Qiu, H. and Lu, Y. (2016), "Flexural behaviour of timber dovetail mortise-tenon joints", *Construct. Build. Mater.*, **112**,

- 366-377. <https://doi.org/10.1016/j.conbuildmat.2016.02.074>.
- Chen, L., Li, S., Wang, Y., Zhao, Y., Zhang, M., Song, X., Li, X., Wu, T. and Jiang, L. (2017), "Experimental study on the seismic behaviour of mortise-tenon joints of the ancient timbers", *Struct. Eng.*, **27**(4), 512-519. <https://doi.org/10.2749/222137917X14881937844720>.
- Chen, Z. (2011), "Behaviour of typical joints and the structure of Yingxian Wood Pagoda", Ph.D. Dissertation, Harbin Institute of Technology, Harbin, China.
- Chun, Q., Yue, Z. and Pan, J. (2011), "Experimental study on seismic characteristics of typical mortise tenon joints of Chinese southern traditional timber frame buildings", *Sci. China Technol. Sci.*, **54**(9), 2404-2411. <https://doi.org/10.1007/s11431-011-4448-3>.
- Cui, Y. (2015), "The finite element analysis of the hysteretic behavior of mortise-tenon joints and frames in ancient timber buildings", Master Dissertation, Xi'an University of Architecture and Technology, Xi'an, China.
- Fang, D., Iwasaki, S., Yu, M., Shen, Q., Miyamoto, Y. and Hikosaka, H. (2001), "Ancient Chinese timber architecture. I: Experimental study", *J. Struct. Eng.*, **127**(11), 1348-1357. [https://doi.org/10.1061/\(asce\)0733-9445\(2001\)127:11\(1348\)](https://doi.org/10.1061/(asce)0733-9445(2001)127:11(1348)).
- GB 50165-92 (1992), Technical code for maintenance and strengthening of ancient timber buildings, China Architecture and Building Press; Beijing, China.
- GB/T 1929-09 (2009), Method of sample logs sawing and test specimens selection for physical and mechanical tests of wood, Standard Press of China; Beijing, China.
- Guo, T. (2016), "Experimental study on the seismic behavior of traditional Chuan-Dou style wood frame", Master Dissertation, Chongqing University, Chongqing, China.
- Hao, X. (2015), "An experimental study on the structural performance of beam-lifted frame and through type frame", Master Dissertation, Southeast University, Nanjing, China.
- Li, Y., Cao, S. and Xue, J. (2016), "Analysis on mechanical behavior of dovetail mortise-tenon joints with looseness in traditional timber buildings", *Struct. Eng. Mech.*, **60**(5), 903-921. <https://doi.org/10.12989/sem.2016.60.5.903>.
- McKenzie, W. and Karpovich, H. (1968), "The frictional behaviour of wood", *Wood Sci. Technol.*, **2**(2), 139-152. <https://doi.org/10.1007/BF00394962>.
- Meng, X., Yang, Q., Wei, J. and Li, T. (2018), "Experimental investigation on the lateral structural performance of a traditional Chinese pre-Ming dynasty timber structure based on half-scale pseudo-static tests", *Eng. Struct.*, **167**, 582-591. <https://doi.org/10.1016/j.engstruct.2018.04.077>.
- Murase, Y. (1984), "Friction of wood sliding on various materials", *J. Faculty Agriculture Kyushu U.*, **28**(4), 147-160. <https://doi.org/10.1021/jf00126a056>.
- Pan, W., Xue, J. and Bai, Y. (2017), *Seismic Performance and Reinforcement Design Method of Civil Structure Dwellings*, Science Press, Beijing, China.
- Qu, Z., Dutu, A., Zhong, J. and Sun, J. (2015), "Seismic Damage to Masonry-Infilled Timber Houses in the 2013 M7.0 Lushan, China, Earthquake", *Earthq. Spectra*, **31**(3), 1859-1874. <https://doi.org/10.1193/012914EQS023T>.
- Vieux-Champagne, F., Sieffert, Y., Grange, S., Nko'ol, C., Bertrand, E., Duccini, J., Faye, C. and Daudeville, L. (2017), "Experimental analysis of a shake table test of timber-framed structures with stone and earth infill", *Earthq. Spectra*, **33**(3), 1075-1100. <https://doi.org/10.1193/010516EQS002M>.
- Xie, Q., Wang, L., Zheng, P., Zhang, L. and Hu, W. (2018), "Rotational behavior of degraded traditional mortise-tenon joints: experimental tests and hysteretic model", *J. Architectural Heritage*, **12**(1), 125-136. <https://doi.org/10.1080/15583058.2017.1390629>.
- Xue, J., Qi, L., Yang, K. and Wu, Z. (2017), "Dynamic

- experimental study on single and double beam-column joints in steel traditional-style buildings”, *Struct. Eng. Mech.*, **63**(5), 617-628. <https://doi.org/10.12989/sem.2017.63.5.617>.
- Xue, J. and Xu, D. (2018), “Shake table tests on the traditional column-and-tie timber structures”, *Eng. Struct.*, **175**, 847-860. <https://doi.org/10.1016/j.engstruct.2018.08.090>
- Xue, J., Xu, D. and Qi, L. (2019), “Experimental seismic response of a column-and-tie wooden structure”, *Adv. Struct. Eng.*, **22**(8), 1909-1922. <https://doi.org/10.1177/1369433219828647>
- Yeo, S., Hsu, M., Komatsu, K., Chung, Y. and Chang, W. (2016), “Shaking table test of the Taiwanese traditional Dieh-Dou timber frame”, *J. Architectural Heritage*, **10**(5), 539-557. <https://doi.org/10.1080/15583058.2015.1009574>.
- Yeo, S., Komatsu, K., Hsu, M., Chung, Y. and Chang, W. (2018), “Structural behavior of traditional Dieh-Dou timber main frame”, *J. Architectural Heritage*, **12**(4), 555-577. <https://doi.org/10.1080/15583058.2018.1442518>.
- Yue, Z. (2014), “Traditional Chinese wood structure joints with an experiment considering regional differences”, *J. Architectural Heritage*, **8**(2), 224-246. <https://doi.org/10.1080/15583058.2012.688179>.
- Zhang, W. (2019), “The seismic and lateral resistance of column-and-tie wooden buildings based on mortise-tenon joint”, *Wood Products J.*, **10**(2), 86-91. <https://doi.org/10.1080/20426445.2019.1636520>
- Zhang, X., Xue, J., Zhao, H. and Sui, Y. (2011), “Experimental study on Chinese ancient timber-frame building by shaking table test”, *Struct. Eng. Mech.*, **40**(4), 453-469. <http://dx.doi.org/10.12989/sem.2011.40.4.453>.
- Zhao, H., Xue, J. and Sui, Y. (2012), *Structure and Seismic Resistance of Chinese Ancient Buildings: Test, Theory and Strengthening Method*, Science Press, Beijing, China.
- Zhuang, Z., You, X., Liao, J., Cen, S., Shen, X. and Liang, M. (2009), *Finite Element Analysis and Application Based On ABAQUS*, Tsinghua University Press, Beijing, China.